Comparison of Oxygen Adsorption and Platinum Dissolution in Acid and Alkaline Solutions Using Electrochemical Quartz Crystal Microbalance

ChemElectroChem

Research Article
doi.org/10.1002/celc.202200591

Chemistry Europe
European Chemical Societies Publishing

www.chemelectrochem.org

Comparison of Oxygen Adsorption and Platinum Dissolution in Acid and Alkaline Solutions Using Electrochemical Quartz Crystal Microbalance

Linnéa Strandberg,*[a] Victor Shokhen,[a, b] Mathilde Luneau,[a] Göran Lindbergh,[c] Carina Lagergren,[c] and Björn Wickman*[a, b]

Platinum (Pt) is a widely used electrocatalyst material in fuel cells and electrolysers. Proton exchange membrane (PEM) fuel cells and electrolysis operate under highly acidic conditions whereas the more recently developed anion exchange membrane (AEM) processes take place under alkaline conditions. Pt dissolution and Pt oxidation during operation and varying potentials has been studied mainly for the acidic PEM and less for the alkaline AEM. This study presents a comparison of Pt dissolution and Pt oxidation in 0.5 M H_2SO_4 and 1 M KOH using electrochemical quartz crystal microbalance (EQCM) on Pt thin films. Physical characterisation using electron microscopy and atomic force microscopy (AFM) revealed small, yet significant differences in the Pt film surface structure, which is related to differences in measured electrochemical surface area (ECSA). The mass increase from adsorption of oxygenated species and Pt oxidation is higher in alkaline conditions compared to in acid while dissolution of Pt is similar.

Introduction

To reduce climate gas emissions, our society needs to move away from energy systems reliant on carbon based energy carriers such as fossil fuel to eco-friendly alternative energy systems, such as the hydrogen economy.[1–3] Electrolysers and fuel cells are used to convert electricity to H_2 and H_2 to electricity, respectively. In both applications, efficient catalysts are required to make hydrogen a more competitive alternative. The platinum group metals are often used in commercial applications due to their stability and efficiency, although they have some limitations and challenges.[4] Although platinum (Pt) is considered a stable element, it slowly degrades over time during the electrocatalytic reactions, especially during reactions such as oxygen reduction/evolution reaction (ORR and OER).[5] These reactions cause the Pt to dissolve and redeposit, in a process called Oswald ripening, which over time will lead to a loss of active surface area and reduces the electrochemical activity.

[a] L. Strandberg, Dr. V. Shokhen, Dr. M. Luneau, Prof. B. Wickman
Department of Physics
Chalmers University of Technology
41296, Göteborg, Sweden
E-mail: linnea.strandberg@chalmers.se
bjorn.wickman@chalmers.se
[b] Dr. V. Shokhen, Prof. B. Wickman
Competence Center for Catalysis
Chalmers University of Technology
41296, Göteborg, Sweden
[c] Prof. G. Lindbergh, Prof. C. Lagergren
Department of Chemical Engineering
KTH Royal Institute of Technology
10044, Stockholm, Sweden

The lifetime of fuel cell components needs to be increased,[6] and for that reason, many studies focused on the degradation mechanism of Pt in acidic conditions as these are the relevant conditions used in the established proton exchange membrane (PEM) fuel cells (FCs) and electrolysis cells (ECs).[7]

With the rise of anion exchange membrane (AEM) technologies, AEMFCs and AEMECs have the potential to overcome some of the disadvantages of PEM technologies, such as less harsh condition allowing for non-noble catalyst and long-term stability.[4] Degradation in alkaline environment has been less studied than degradation in acidic environment, and more work needs to be done within that area.

Pt can be degraded through dissolution into the electrolyte when Pt oxide is being reduced, leading to mass loss and surface restructuring. One in-situ technique that can be used to study the degradation of electrodes is an inductively coupled plasma mass spectrometer (ICP-MS) coupled to an electrochemical cell.[8,9] With a half-cell setup connected to ICP-MS, Topalov et al. found that Pt degradation usually begins by dissolving into the electrolyte during the cathodic sweep after the anodic sweep, in the oxide reduction potential region and at potentials above 1 V vs. reversible hydrogen electrode (RHE).[8]

Zhongqi et al. measured the Pt dissolution in alkaline condition of KOH using ICP-MS, while cycling the potential between 0.4 and 1.4 V_{RHE}.[10] The results show similar behaviour as in acidic condition, where Pt is mostly dissolved during cathodic sweeps, when the Pt-oxide is being reduced, with dissolution starting at an upper potential limit (UPL) of above 1.0 V_{RHE}.

Another in-situ method to investigate material mass change is quartz crystal microbalance (QCM). With QCM, the mass change is observed by measuring the frequency shift of a

quartz crystal resonator.[11] QCM combined with electrochemical measurements (EQCM), can be used to measure stability and degradation in form of mass loss from an electrode during electrochemical reactions,[12–14] or to measure the mass of surface species adsorbed during electrochemical cycling which Jerkiewicz et al. have done for Pt in acidic solutions.[15,16] The underlying principle for using EQCM is that the Pt mass at the electrode changes with potentials. When a potential is applied to Pt, especially when the potential is swept above the Pt oxidation potential of $E > 0.7\ V_{RHE}$, mass is gained due to adsorption of oxygenated species such as Pt–O and Pt–OH and surface oxidation. Likewise, during cathodic sweeps the reduction of the Pt surface back to its metal state results in a reduction of mass. Moreover, mass changes between the start of each sweep indicate that the surface has been permanently affected by the process. At low potentials, $0 < E < 1.0\ V_{RHE}$, the dissolution rate of Pt in acidic conditions is negligible, whereas at higher potentials, $E > 1.0\ V_{RHE}$, the Pt begins to dissolve into Pt^{2+} during cathodic sweeps. These ions can later redeposit back to other locations on the surface.

It is unclear if results from studies in acidic media can be translated to alkaline media, and comparison between existing studies of Pt in different media are made difficult since differences in manufacturing methods can result in variations in surface structures and electrochemical surface area (ECSA), which can skew the results. Therefore, more work needs to be done to further investigate the behaviour of Pt under alkaline conditions, and how it differs from acidic conditions.

In this work, EQCM measurements of Pt thin films during cyclic voltammetry (CV) are presented for different UPLs in acidic and alkaline electrolytes. Measurements were done using identical samples in both electrolytes, as well as using the same sample for measurements in both electrolytes. Furthermore, the effects of cycling on the surfaces' morphology are examined using a combination of scanning electron microscopy (SEM), transmission electron microscopy (TEM) and atomic force microscopy (AFM). EQCM shows a difference in how the mass changes during each cycle in alkaline vs. acidic electrolyte, with more mass being gained during oxidation in alkaline environment compared to an acidic environment. The mass lost during cycling was found to be dependent on UPL, but not on electrolyte. The ECSA obtained using H_{UPD} was larger when measured in acidic environments. Results from SEM, TEM and AFM shows that the surface differs depending on which electrolyte the sample has been exposed to during cycling.

Results and Discussion

The influence of pH on the mass response of a Pt thin film was investigated during electrochemical measurements using QCM samples in two different conditions: i) in an acidic solution and ii) in an alkaline solution.

EQCM measurements in acidic conditions

The CVs measured in 0.5 M H_2SO_4 show the characteristic features of a pure poly-crystalline Pt surface and the corresponding mass response for different UPLs are in agreement with previous reported data (Figure 1a).[15]

The mass is only measured in terms of change and does not have a set absolute value. Therefore, the baseline for the mass shift is set as the mass at the start of each cycle if not otherwise stated. The ECSAs of different samples, as calculated from the hydrogen adsorption/desorption region, are in the span of 1.00 to 1.14 cm^2, corresponding to a roughness factor R of about 4.4 to 5.0 which is within the range of previous reported values for Pt thin films.[17] The ECSAs were also measured with CO-stripping, yielding similar results (Table 1).

The mass response can be divided into four parts with corresponding regions in the CV: The hydrogen adsorption/desorption region in 0.05 to 0.4 V_{RHE}, the double layer region between 0.4 and 0.6 V_{RHE}, the oxidation region during the

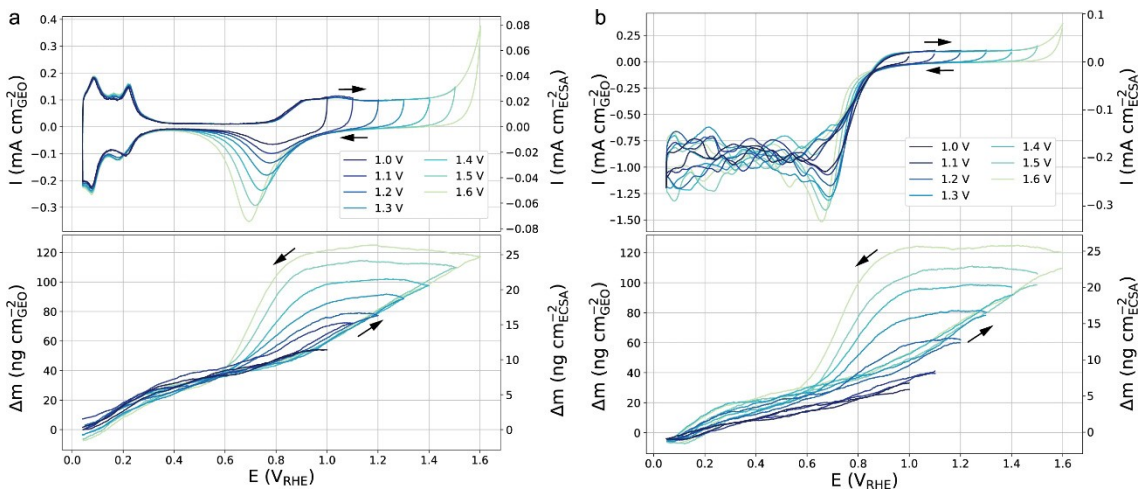

Figure 1. CVs and corresponding mass response for different UPL for Pt in 0.5 M H_2SO_4 in Ar-saturated electrolyte (a) and O_2-saturated electrolyte (b). Measurements were performed at room temperature with a scan speed of 50 mV s^{-1}.

anodic scan from 0.8 V_{RHE} to UPL and the reduction region during the cathodic scan from UPL to 0.6 V_{RHE}. In the hydrogen region the mass increases as hydrogen desorbs and decreases again when the hydrogen is adsorbed. This is caused by water molecules being displaced from the surface as hydrogen is adsorbed.[18–20] In the double layer region, the mass increases slowly as the voltage is increased. This is caused by anion adsorption and H_2O physisorption.[20] The onset of oxidation of Pt in the CV at 0.8 V_{RHE} corresponds to an increase in the slope of the mass gain, which then stays constant until the scan direction is reversed. During the cathodic scan, the mass stays roughly constant until the onset of reduction of oxidised Pt at about 0.9 V_{RHE}, after which the mass decreases steadily until all Pt oxide has been reduced, at about 0.6 V_{RHE}. The mass at 0.6 V_{RHE} is slightly lower during cathodic scan than the anodic scan, indicating that some mass has been lost during the oxidation/reduction process. The mass gained in the oxide region during the anodic scan (Figure 1) scales linearly with the UPL, indicating that the amount of oxide formed increases linearly with the UPL as well.

The CV and mass response were also measured for O_2-saturated H_2SO_4 (Figure 1b). The CV shows clear signs of oxygen reduction taking place at $E < 0.8$ V_{RHE}. However, this does not appear to translate in a change in the mass response. The mass responses are similar to the ones measured in deoxygenated electrolyte, indicating that the Pt–OH/Pt–O formation does not depend on the concentration of O_2 in the electrolyte, but rather that OH adsorption and Pt oxidation is caused by reactions with water.

Although we in this work focus on 0.5 M H_2SO_4 as our acidic electrolyte, similar to previous publications,[16,21] a comparison with 0.1 M $HClO_4$ was made to see how the mass response is affected by different acidic electrolytes. 0.1 M $HClO_4$ is a commonly used benchmarked acidic electrolyte often used e.g. in evaluation of oxygen reduction reaction catalysts.[22–24] As can be seen in Figure 2a and b, no major difference in mass response could be discerned between measurements done in H_2SO_4 and $HClO_4$.

EQCM measurements in alkaline conditions

To see how alkaline conditions affect the mass change on a Pt surface, electrochemical measurements were done in 1 M KOH. CVs and corresponding mass responses were measured for different UPLs in Ar-saturated 1 M KOH (Figure 3 a). As with the acidic mass response, (Figure 1a), the mass change can be divided into four regions corresponding to the hydrogen adsorption/desorption at 0.05 V_{RHE} to 0.4 V_{RHE}, the double layer region between 0.4 V_{RHE} and 0.7 V_{RHE}, the oxidation region in 0.7 V_{RHE} to UPL and the reduction region in UPL to 0.6 V_{RHE} in the CVs.

Unlike the acidic case, where the mass increases continuously from 0.05 V_{RHE}, in alkaline electrolyte the mass stays roughly constant below 0.2 V_{RHE}, and between 0.2 V_{RHE} and 0.4 V_{RHE} the mass increases when hydrogen desorbs and decreases when hydrogen adsorbs. In the double layer region, the mass increases slightly. From 0.7 V_{RHE}, at the onset of Pt–OH formation, to the UPL, the mass increases constantly. During the cathodic scan, the mass decreases slowly from UPL down to ca 0.9 V_{RHE} corresponding to the onset of Pt–O reduction in the CV, after which the mass decreases more rapidly until most Pt oxide has been reduced at 0.6 V_{RHE}. During cycling, the mass at 0.6 V_{RHE} is higher before the oxidation/reduction cycle has taken place, indicating that Pt atoms are lost from the surface during reduction which is in agreement with previous studies.[8]

In O_2-saturated KOH, the CVs show that oxygen is being reduced, and much like in the acidic case, the mass response is

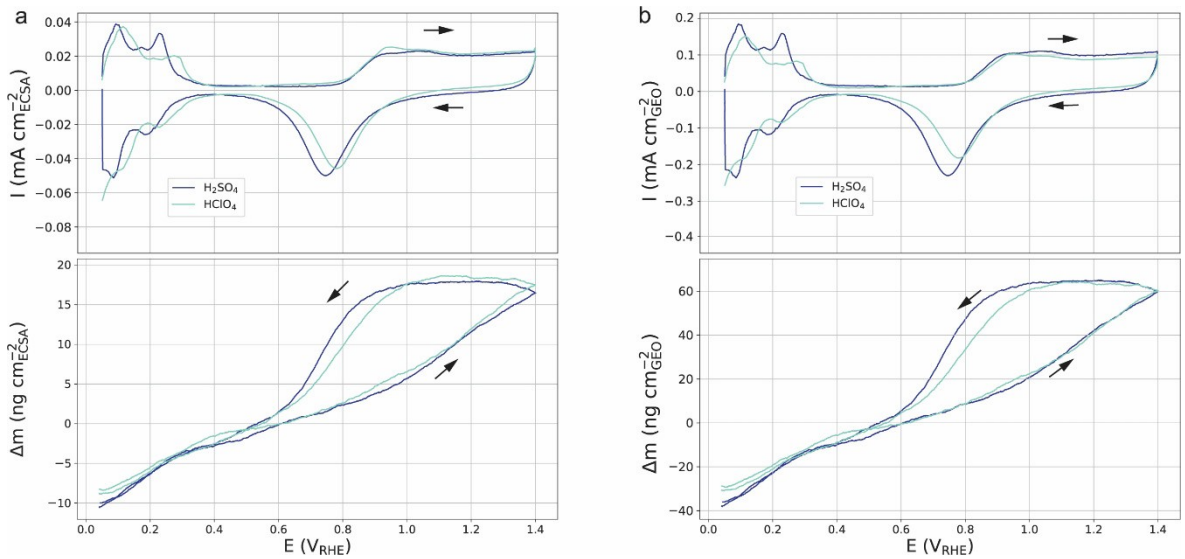

Figure 2. A comparison of a CVs and corresponding mass response for different UPLs for Pt in 0.5 M H_2SO_4 (dark blue) and 0.1 M $HClO_4$ (light blue) normalised per ECSA (a) and geometrical surface area (b). Measurements were performed on the same crystal at room temperature with a scan speed of 50 mV s^{-1} and the electrolyte was saturated with Ar. The mass baseline was set at 0.6 V_{RHE} to facilitate the distinction of differences of the data sets in oxidation/reduction region and the double layer/hydrogen region.

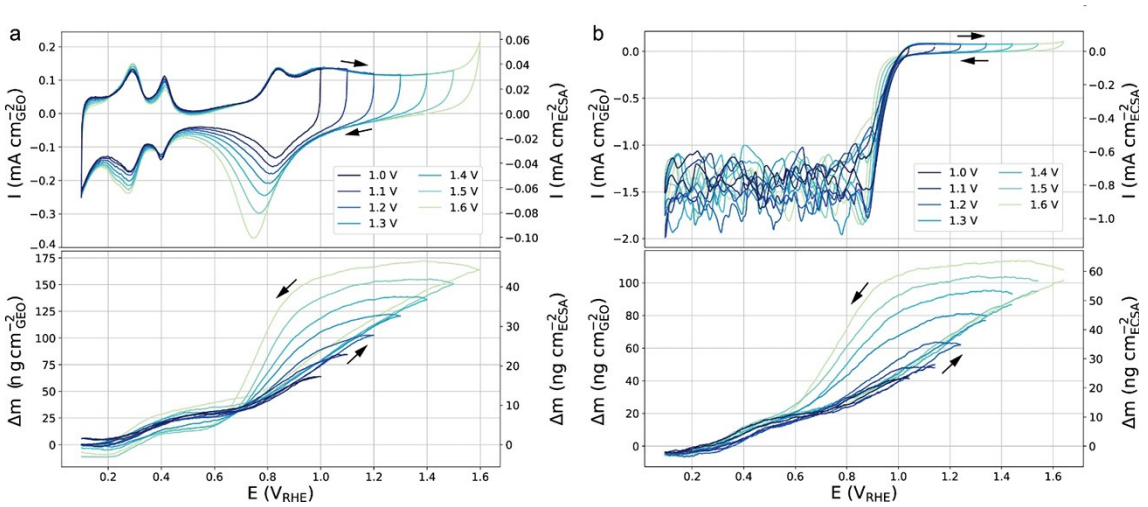

Figure 3. CVs and corresponding mass response for different UPL for Pt in 1 M KOH in Ar-saturated electrolyte (a) and O_2-saturated electrolyte (b). Measurements were performed at room temperature with a scan speed of 50 mV s^{-1}.

similar to that measured in Ar-saturated KOH although the total amount of mass gained is less in O_2 than in the Ar-saturated electrolyte (Figure 3b). This indicates that the oxygen concentration in the electrolyte has no significant impact on the mass change of the surface and that a high concentration of O_2 does not increase oxidation of the surface during CV.

ECSA as measured by H_{UPD} was 0.760 cm^2, corresponding to a roughness of R = 3.35, which is about 75% of the ECSA measured in H_2SO_4. This discrepancy in ECSA was consistent between different samples. To check whether the difference could be due to natural variances between the crystals, the ECSA was measured on the same crystal in both alkaline and acidic electrolyte. The difference measured in ECSA was present, with the measured area in alkaline media being around 80% of that measured in acidic media. Furthermore, the ECSA was also measured using CO-stripping, yielding similar results (Table 1).

Table 1. Roughness factors (ECSA / geometrical area) for different samples as measured after initial cycling in 1 M KOH and 0.5 M H_2SO_4. Measurements marked α and β were done on the same crystal in both 1 M KOH and 0.5 M H_2SO_4.

Electrolyte	Roughness factor CO-stripping	Roughness factor H_{UPD}	Notes
1 M KOH	3.88	3.30	α
	4.13	3.69	β
	3.26	3.01	
	4.21	4.04	
	4.10	3.52	
	4.14	3.80	
0.5 M H_2SO_4	4.32	4.43	α
	4.51	4.65	β
	4.35	4.54	
	4.35	4.63	
	4.56	4.80	
	4.77	5.05	

Mass loss

In both acidic and alkaline measurements, Pt is lost during cycling and the mass loss depends on UPLs (Figure 4a and b). The amount of mass loss increases with UPL, which can be due to the fact that at higher UPLs the Pt oxide layer becomes thicker, and more Pt is dissolved into the electrolyte when reduced rather than recrystallising on the surface. At an UPL of 1.0 V_{RHE}, close to no mass is lost between cycles, and the film is stable. At an UPL of 1.1 V_{RHE} circa 2 ng cm$^{-2}_{ECSA}$ cycle^{-1} is lost during cycling, indicating that dissolution is taking place, and at an UPL of 1.6 V_{RHE} the mass is reduced by around 7 ng cm$^{-2}_{ECSA}$ cycle^{-1} for both samples. This is in very good agreement with previously reported data measured using ICP-MS.[8,25,26]

Comparison between acid and alkaline environment

The mass response of one crystal was measured in both H_2SO_4 and KOH for UPL = 1.4 V (Figure 5a) yet after electrochemical annealing, different electrochemical surface area was measured in the two electrolytes. When normalised to geometrical surface area, 15% more mass is gained during oxidation in alkaline electrolyte. When comparing mass change per ECSA, the difference in mass gained during oxidation becomes much more pronounced with about 45% more mass gained in the oxide region in alkaline conditions compared to acidic conditions. Furthermore, the mass response in the hydrogen region is different between alkaline and acidic electrolyte, with mass being gained in alkaline media while mass is lost in acidic media.

Jerkiewicz et al. found that when extending the cycling window to lower potentials in H_2SO_4, the mass reaches a minimum at around 0.045 V_{RHE}, after which the mass increase again, and they attribute this potential of minimum mass to the

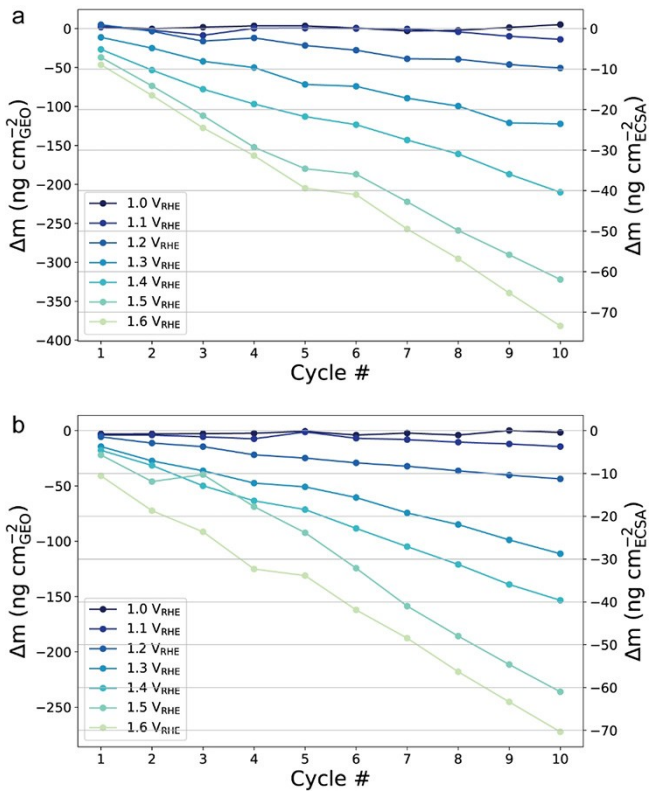

Figure 4. Cumulative mass loss per cycle for different UPLs in a) 0.5 M H_2SO_4 and b) 1 M KOH. The mass change is measured relative to the starting mass of the first cycle.

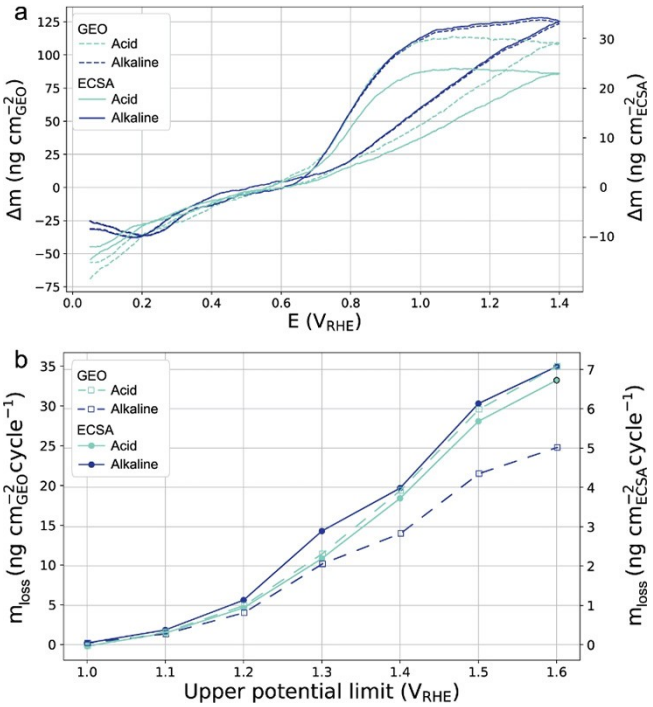

Figure 5. a) Comparison of mass change in 0.5 M H_2SO_4 and 1 M KOH normalised to the geometrical surface area (dashed lines) and ECSA (solid lines). The measurements were done on the same crystal in room temperature. The electrolyte was saturated with Ar. b) Average mass lost per cycle for different UPLs in alkaline (dark blue) and acidic electrolyte (light blue) normalised to geometric surface area (dashed lines/squares) and ECSA (solid lines/circles).

potential at which a complete layer of hydrogen has been adsorbed.[16] Our results indicate that Pt has a higher point of lowest mass in alkaline solution, at ca 0.2 V_{RHE}, which coincides with the peak of hydrogen adsorption in the CV. Moreover, the reduction of mass starts earlier in KOH, with a slow mass loss from UPL down to ca 0.9 V_{RHE} and a faster mass loss between 0.9 V_{RHE} and 0.6 V_{RHE}, rather than plateauing from UPL until ca 0.9 V_{RHE} as in the acidic case.

When comparing mass loss per cycle, (Figure 5b), 40% more mass is lost each cycle at UPL = 1.6 V_{RHE} in acid compared to alkaline per geometrical surface area. However, when normalised to ECSA, the difference is much smaller, with 5% more mass being lost each cycle in alkaline conditions, and the trend follows a similar pattern in both acidic and alkaline conditions. This indicates that the measured differences in ECSA are correlated to real behaviour of the Pt surface, and that Pt has similar dissolution rates in high and low pH electrolytes.

It is important to note that we assume the same surface charge and coverage when calculating the ECSA in either electrolyte, based on an average surface charge of 210 $\mu C\,cm^{-2}$ of the most common crystal facets and a surface coverage of 77% at the distinct local maximum before hydrogen evolution starts used as integration limit.[27] While many use the same surface charge for alkaline media,[28,29] some use a different conversion factor when measured in KOH.[30,31] This could be interpreted as Pt in alkaline conditions having a different surface coverage of hydrogen at the local maximum, perhaps due to blocking of sites by ions. Such a difference could explain parts of the discrepancy in measured ECSA. Another possibility is that Pt thin films have physically different surface structures in KOH and H_2SO_4. After the crystals have been inserted into the electrolyte, they are electrochemically annealed (cycled), which changes the surface. Possibly this process can have different effects on the surface structure whether it is performed in alkaline or acidic media, which could help explain the discrepancies in ECSA. Therefore, physical characterisation was performed on three different crystals, one fresh, one treated electrochemically in 0.5 M H_2SO_4 and one in 1 M KOH, to study any potential differences in surface morphology.

Physical characterization

Atomic force microscopy

AFM images were taken of the Pt surface on the quartz crystals of one fresh sample, one sample that has been cycled in 0.5 M H_2SO_4 and one sample that has been cycled in 1 M KOH (Figure 6). In AFM, the sample treated with acid shows a Ra-roughness of 1.034, compared to alkaline treated sample with a roughness of 1.027 and the fresh sample with a roughness of 1.026. AFM shows only larger features and not smaller particles and cracks on the atomic scale, both of which contribute to the

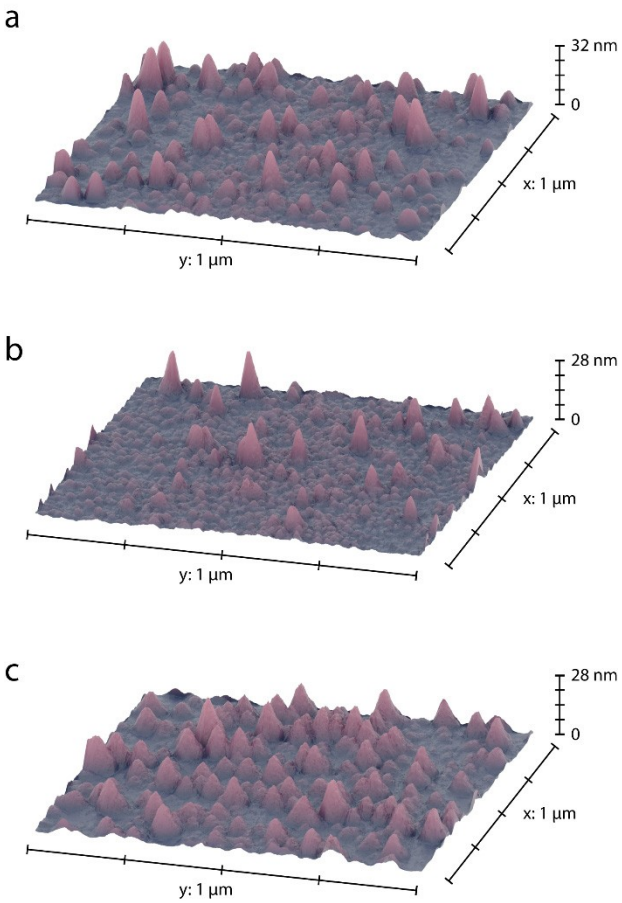

Figure 6. AFM images of a) fresh Pt thin film b) Pt film after measurements in acid and c) Pt film after measurements in alkaline.

electrochemical surface area. For that reason, the roughness measured with AFM is much smaller than that measured with ECSA. Even so, AFM shows that the acid-treated sample has a slightly larger surface area than the alkaline-treated sample, in congruence with the measured ECSAs. A change in the surface morphology could, at least partly, explain the different ECSAs measured.

Electron microscopy

SEM images of the fresh sample show a rough homogeneous Pt surface coated on the QCM substrate (Figure 7a). The surface post reaction in acidic and alkaline electrolytes have slightly different texture and roughness (Figures 7b and c). The lower images represent a higher magnification of the SEM images.

Figure 8a shows representative TEM images of a cross section of the surface of a fresh sample, and Figures 8b–c present the changed Pt structure post acidic and alkaline electrochemical procedure. For all samples, similar surface structures were seen throughout the whole cross-sectional surface. The cross-section area of Pt shows up as the dark region, while the lighter grey region is the amorphous protective layer of Nafion. The cross-section view reveals that the roughness of the surfaces of the samples were changed similarly to AFM. Within the post-acidic structure (Figure 8b), the bright stains are inner cracks that were formed inside the Pt structure. However, after the alkaline electrochemical procedure (Figure 8c), the inner structure is left solid as for the fresh sample.

Higher magnification images of the samples (Figure 8, middle row) reveal the atomic fringes of an average Pt bump projected outward the surface. The fresh Pt sample shows a smooth bump structure, whereas, in both post electrochemical procedures, Pt has a more deformed structure. Fast Fourier

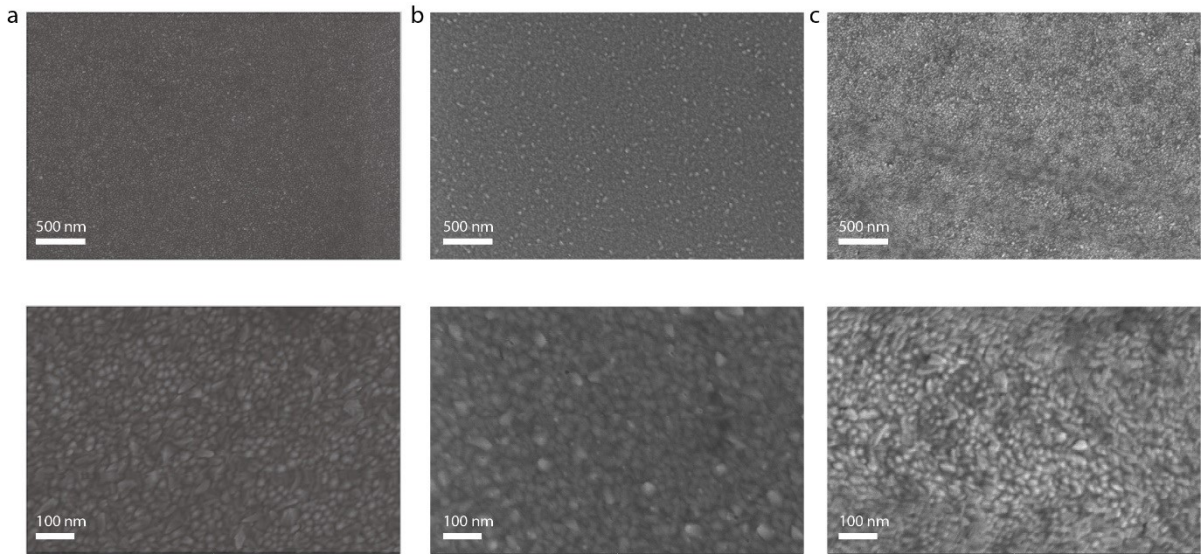

Figure 7. SEM images of EQCM samples of a) a fresh sample, b) an H_2SO_4 treated sample and c) a KOH treated sample. Upper image shows an overview and lower image a zoom in.

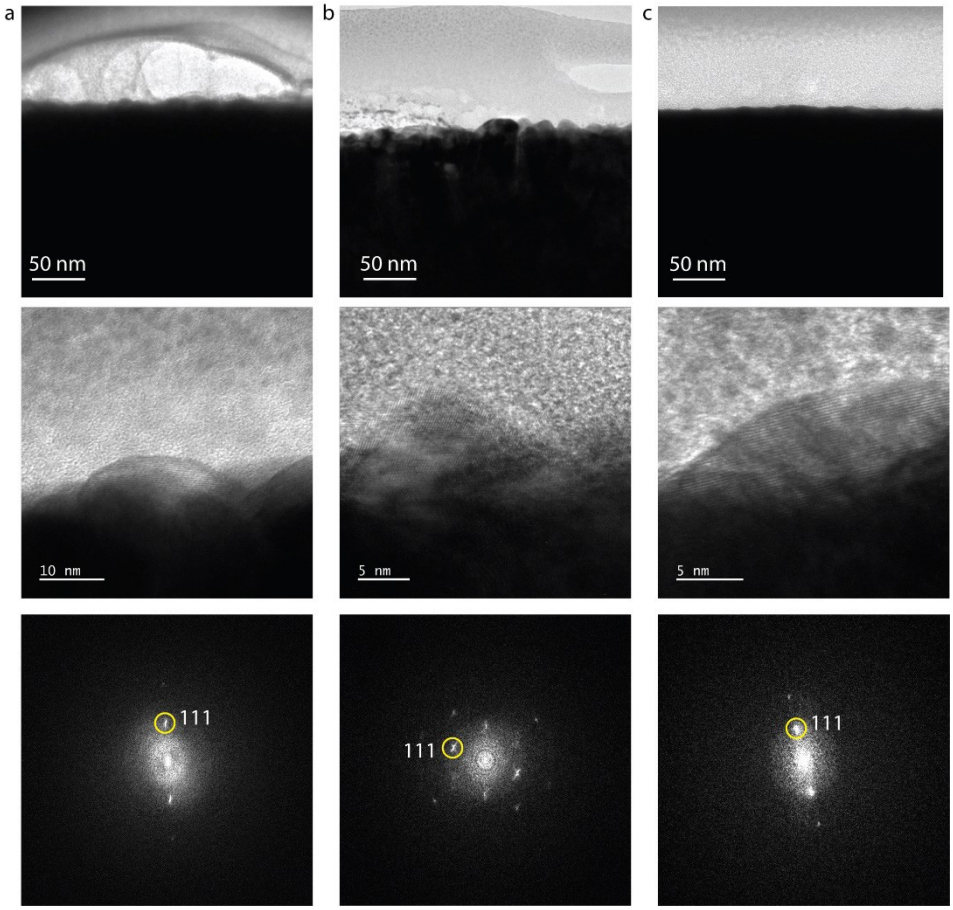

Figure 8. TEM images of EQCM samples of a) a fresh sample, b) an H_2SO_4 treated sample and c) a KOH treated sample. Upper image shows an overview, the middle image shows a zoom in, and the lower image shows the corresponding FFT image.

transform (FFT) images of the bumps reveal different d-spacing (Figure 8, lower row). All the samples reveal regular Pt structure d-spacing of 2.27 Å and 1.97 Å suitable for Pt Millar indexes $<111>$ and $<200>$, respectively (COD 1011109). However, post electrochemical reaction the surface is more deformed.

Conclusions

EQCM measurements on Pt thin films in 1 M KOH and 0.5 M H_2SO_4 show a difference in mass response during cyclic voltammetry. Different ECSAs were measured depending on electrolyte, with the ECSA measured in KOH tending to be ca 75–80% of the ECSA measured in H_2SO_4. The amount of mass gained during oxidation of Pt is larger in alkaline than in acid, and that difference gets larger when normalised to ECSA. Mass loss per cycle increased with UPL, and, when normalised to ECSA, showed similar amount of dissolution in KOH and H_2SO_4. No mass was lost during cycling at UPL ≤ 1 V_{RHE}. TEM imaging showed differences in surface morphology after cycling in KOH vs. H_2SO_4, which could in part explain the differences in ECSA.

Our results elucidate some of the similarities and differences of the behaviour of Pt in alkaline and acidic conditions, which is of value for fundamental understanding of electrochemical behaviour of Pt in acid and alkaline environments, and needed with the rise of AEM based technologies.

Experimental Section

EQCM measurements

Cyclic voltammetry was measured using a SP-300 potentiostat from Biologic controlled by Biologic's EC-labb software. EQCM measurements were performed using a dip holder from MicroVacuum connected to a QSense Explorer frequency response analyser from Biolin Scientific with an in-house built adapter. The QCM data was recorded with the QSoft401 software from Biolin Scientific, which tracks the peak position of the fundamental frequency and its over-frequencies. The dip holder, made from PEEK, was sealed using O-rings made from FFPM and assembled using nylon screws.

The working electrode was made on custom ordered AT-cut quartz crystals from Biolin Scientific with the back side pre-coated with a gold electrode. On the other side, the crystal was coated with a thin film of Pt (200 nm thick) on a Ti underlayer (3 nm thick), both made using Lesker PVD 225 Evaporator from Kurt J. Lesker Company, with a geometrical surface area of 0.227 ± 0.003 cm^2. The quartz crystal is only sensitive to the area where the gold and working electrode overlap, which has an area of 0.197 cm^2.

Before deposition, the crystals were cleaned by sonication in acetone (Sigma-Aldrich), isopropanol (VWR) and Milli-Q water (18.2 MΩ cm) consecutively for ten minutes. They were finally dried with nitrogen, N_2, of grade N6.0 from Strandmöllen.

The crystal has a fundamental frequency of ca 4.95 MHz and the shift in frequency was measured with an accuracy of ± 0.1 Hz, corresponding to a mass change of less than ± 0.4 ng cm^{-2}.

The measurements were done in either 1 M KOH made with suprapur KOH from Merck KGaA and Milli-Q water, using a Hg/HgO reference electrode, type CHI 152, from CH Instruments, 0.5 M H_2SO_4 made with suprapur H_2SO_4 from Merck KGaA and Milli-Q water, or in 0.1 M $HClO_4$ made using suprapur $HClO_4$ from Merck KGaA and milli-Q water, using either a Ag/AgCl reference electrode, B-3420+, or a Hg/Hg_2SO_4 electrode, B-3610+, both from SI Analytics. These concentrations should give a theoretical value of the pH of 14, 0.3 and 1.0 for KOH, H_2SO_4 and $HClO_4$, respectively, and it was confirmed that the real pH of the electrolytes was near these values by measuring the reversible hydrogen electrode (RHE) potential in an experiment where a Pt wire was cycled at 5 mV/s in H_2 saturated electrolyte at potentials close the RHE. The RHE potential vs. the used reference electrode was noted as the intercept of the current axis, and the pH was then calculated with Eq. 1

$$E = E_0 + \mathrm{pH} \times 2.303RT/F \quad (1)$$

where E is the measured potential of where the current crosses zero, E_0 is the known value of the reference electrode relative to RHE at standard conditions, R is the universal gas constant, T is the absolute temperature and F is the Faraday constant. All potentials in this paper are converted to, and presented against, the reversible hydrogen electrode. A 3 mm graphite rod type 496537 from Sigma-Aldrich was used as counter electrode in both set-ups, and the electrolytes were saturated with either Ar or O_2, both gases from Strandmöllen of grade N6.0 purity.

Prior to the experiments, the Pt films were electrochemically annealed by repeatedly cycling the potential between 0.05 and 1.4 V_{RHE} at 100 mV s^{-1} for 50 cycles until the CV was stable. This produces CVs typical of polycrystalline Pt. The electrochemical surface area was determined both from the H_{UPD} region of the CV and by CO-stripping. From a CV recorded with a sweep rate of 50 mV s^{-1} in Ar-saturated electrolyte, the ECSA was calculated from the charge associated with hydrogen adsorption/desorption, assuming a surface coverage of 77%,[27] and a charge density of 210 μC cm^{-2},[32] common for polycrystalline Pt, and removing the charge associated with double layer charging. The roughness factor was then calculated from comparing the ECSA to the geometrical surface area of the electrode. CO-stripping was performed by holding the WE at a potential of 0.1 V_{RHE} for a total of 30 minutes, with CO being bubbled through the electrolyte for the first 15 min, after which the electrolyte was bubbled with Ar. Thereafter the potential was swept 5 times between 0.1 to 1 V_{RHE} at a scan speed of 100 mV s^{-1}. ECSA was calculated from the CO oxidation peak in the first cycle between 0.5 V_{RHE} and 0.8 V_{RHE} using the second cycle as background and assuming a charge density of 420 μC cm^{-2}. No CO oxidation was observed during the second cycle, indicating that all adsorbed CO had reacted.

All measurements were performed at room temperature (293.5 K), with either Ar or O_2 bubbling through the electrolyte. The potential was scanned at a rate of 50 mV s^{-1} from a lower potential of 0.05 V to an upper potential limit (UPL) between 1.0 V and 1.6 V, 10 times for each UPL. The lower potential limit was chosen so that the measurements include the complete hydrogen under potential deposition while avoiding hydrogen evolution, and the UPL ranges from the beginning of oxide formation, up to the beginning of O_2 evolution. The IR drop was compensated to 85% during experiments with the built-in function ZIR in EC-lab, and the remaining 15% was compensated afterwards during data processing.

During the electrochemical measurements, the frequency change of the crystal, defined as the change in peak position from the start of the measurement, was measured for at least three different overtones. The frequency shift, Δf, was converted to a mass shift, Δm, with the Sauerbrey equation[33] (Eq. 2)

$$\Delta m = -\Delta f \frac{\sqrt{\rho_q \mu_q}}{2nf_0^2} \quad (2)$$

where ρ_q is the density of quartz, μ_q is the shear modulus of an AT-cut quartz crystal, f_0 is the initial resonant frequency and n is the number of the harmonic. When using the Sauerbrey equation, it is assumed that the mass change across the electrode surface is homogeneous, that the film is compact, and that the mass change is small compared to the crystal mass. The mass shift from all measured overtones (the 3rd, 5th, 7th and 9th) were averaged. The electrochemical measurements were not started until the frequency had stabilised and did not drift more than 1 Hz per 5 min, corresponding to a mass shift of 0.06 ng s^{-1} which is much smaller than the mass changes of interest.

All glassware and a Teflon cell were cleaned by soaking them in piranha solution (5:1 concentrated sulphuric acid to 30% hydrogen peroxide solution) for at least 3 hours after which they were rinsed 10 times with Milli-Q water. The dip holder and O-rings were cleaned by rinsing them with isopropanol and Milli-Q water.

Physical characterisation

Scanning electron microscopy (SEM) images were taken by SEM Zeiss Ultra 55 FEG.

A focused-ion beam (FIB) (FEI, Versa3D) was used on the QCM samples to prepare lamella slices for cross-section observation by transmission electron microscopy (TEM). To separate the Pt surface from the Pt adhesive layer added during FIB, a protective layer of Nafion was placed on the surface before inserting the samples into the FIB.

TEM images were obtained by High-resolution TEM (HRTEM) using FEI Tecnai G2 F20 operating at 200 kV.

Atomic force microscopy (AFM) images were acquired using a Bruker dimension 3100 scanning probe microscope (SPM).

Acknowledgement

This project is financially supported by the Swedish Foundation for Strategic Research (Project No. ARC19-0026), and by the Swedish Research Council (Project No. 2018-03927). This work was performed in part at Myfab Chalmers and the Chalmers Material Analysis Laboratory, CMAL. The Competence Centre for Catalysis is hosted by Chalmers University of Technology and financially supported by the Swedish Energy Agency and the member companies ECAPS, Johnson Matthey, Perstorp, PowerCell, Preem, Scania CV, Umicore and Volvo Group.

Conflict of Interest

The authors declare no conflict of interest.

Data Availability Statement

The data that support the findings of this study are available from the corresponding author upon reasonable request.

Keywords: Electrochemical quartz-crystal microbalance · Electrochemistry · Platinum · Platinum dissolution · Platinum oxide growth

[1] K. Jiao, J. Xuan, Q. Du, Z. Bao, B. Xie, B. Wang, Y. Zhao, L. Fan, H. Wang, Z. Hou, S. Huo, N. P. Brandon, Y. Yin, M. D. Guiver, *Nature* **2021**, *595*, 361–369.
[2] Z. P. Cano, D. Banham, S. Ye, A. Hintennach, J. Lu, M. Fowler, Z. Chen, *Nat. Energy* **2018**, *3*, 279–289.
[3] Y. Liang, D. McLaughlin, C. Csoklich, O. Schneider, A. S. Bandarenka, *Energy Environ. Sci.* **2019**, *12*, 351–357.
[4] V. R. Stamenkovic, D. Strmcnik, P. P. Lopes, N. M. Markovic, *Nat. Mater.* **2017**, *16*, 57–69.
[5] K. Kodama, T. Nagai, A. Kuwaki, R. Jinnouchi, Y. Morimoto, *Nat. Nanotechnol.* **2021**, *16*, 140–147.
[6] D. A. Cullen, K. C. Neyerlin, R. K. Ahluwalia, R. Mukundan, K. L. More, R. L. Borup, A. Z. Weber, D. J. Myers, A. Kusoglu, *Nat. Energy* **2021**, *6*, 462–474.
[7] R. M. Darling, J. P. Meyers, *J. Electrochem. Soc.* **2003**, *150*, A1523.
[8] A. A. Topalov, I. Katsounaros, M. Auinger, S. Cherevko, J. C. Meier, S. O. Klemm, K. J. J. Mayrhofer, *Angew. Chem. Int. Ed.* **2012**, *51*, 12613–12615; *Angew. Chem.* **2012**, *124*, 12782–12785.
[9] C. Stumm, S. Grau, F. D. Speck, F. Hilpert, V. Briega-Martos, K. Mayrhofer, S. Cherevko, O. Brummel, J. Libuda, *J. Phys. Chem. C* **2021**, *125*, 22698–22704.
[10] Z. Wang, E. Tada, A. Nishikata, *J. Electrochem. Soc.* **2016**, *163*, C853.
[11] Y. Ji, Z.-W. Yin, Z. Yang, Y.-P. Deng, H. Chen, C. Lin, L. Yang, K. Yang, M. Zhang, Q. Xiao, J.-T. Li, Z. Chen, S.-G. Sun, F. Pan, *Chem. Soc. Rev.* **2021**, *50*, 10743–10763.
[12] B. Wickman, H. Grönbeck, P. Hanarp, B. Kasemo, *J. Electrochem. Soc.* **2010**, *157*, B592.
[13] R. Frydendal, E. A. Paoli, B. P. Knudsen, B. Wickman, P. Malacrida, I. E. L. Stephens, I. Chorkendorff, *ChemElectroChem* **2014**, *1*, 2075–2081.
[14] J. Widera, M. Skompska, K. Jackowska, *Electrochim. Acta* **2001**, *46*, 4125–4131.
[15] G. Jerkiewicz, G. Vatankhah, J. Lessard, M. P. Soriaga, Y.-S. Park, *Electrochim. Acta* **2004**, *49*, 1451–1459.
[16] G. Jerkiewicz, G. Vatankhah, S. Tanaka, J. Lessard, *Langmuir* **2011**, *27*, 4220–4226.
[17] W. Visscher, J. F. E. Gootzen, A. P. Cox, J. A. R. Van Veen, *Electrochim. Acta* **1998**, *43*, 533–547.
[18] V. I. Birss, M. Chang, J. Segal, *J. Electroanal. Chem.* **1993**, *355*, 181–191.
[19] M. Osawa, M. Tsushima, H. Mogami, G. Samjeske, A. Yamakata, *J. Phys. Chem. C* **2008**, *112*, 4248–4256.
[20] K. Shimazu, H. Kita, *J. Electroanal. Chem.* **1992**, *341*, 361–367.
[21] J. Kim, P. Urchaga, S. Baranton, C. Coutanceau, G. Jerkiewicz, *Phys. Chem. Chem. Phys.* **2017**, *19*, 21955–21963.
[22] R. Gómez, J. M. Orts, B. Álvarez-Ruiz, J. M. Feliu, *J. Phys. Chem. B* **2004**, *108*, 228–238.
[23] C. C. L. McCrory, S. Jung, I. M. Ferrer, S. M. Chatman, J. C. Peters, T. F. Jaramillo, *J. Am. Chem. Soc.* **2015**, *137*, 4347–4357.
[24] G. A. Kamat, J. A. Zamora Zeledón, G. T. K. K. Gunasooriya, S. M. Dull, J. T. Perryman, J. K. Nørskov, M. B. Stevens, T. F. Jaramillo, *Commun. Chem.* **2022**, *5*, 1–10.
[25] S. Cherevko, A. R. Zeradjanin, G. P. Keeley, K. J. J. Mayrhofer, *J. Electrochem. Soc.* **2014**, *161*, H822.
[26] A. A. Topalov, S. Cherevko, A. R. Zeradjanin, J. C. Meier, I. Katsounaros, K. J. J. Mayrhofer, *Chem. Sci.* **2014**, *5*, 631–638.
[27] T. Biegler, D. A. J. Rand, R. Woods, *J. Electroanal. Chem. Interfacial Electrochem.* **1971**, *29*, 269–277.
[28] D. J. Weber, M. Janssen, M. Oezaslan, *J. Electrochem. Soc.* **2019**, *166*, F66.
[29] J. Li, J. Liu, C. Chen, J. Guo, R. Bi, S. Chen, L. Zhang, M. Zhu, *Chem. Eng. J.* **2022**, *436*, 135186.
[30] F. J. Vidal-Iglesias, R. M. Arán-Ais, J. Solla-Gullón, E. Herrero, J. M. Feliu, *ACS Catal.* **2012**, *2*, 901–910.
[31] C.-L. Sun, J.-S. Tang, N. Brazeau, J.-J. Wu, S. Ntais, C.-W. Yin, H.-L. Chou, E. A. Baranova, *Electrochim. Acta* **2015**, *162*, 282–289.
[32] S. B. Brummer, *J. Phys. Chem.* **1965**, *69*, 562–571.
[33] J. Kankare, *Langmuir* **2002**, *18*, 7092–7094.

Manuscript received: May 30, 2022
Revised manuscript received: August 30, 2022
Accepted manuscript online: September 27, 2022

RESEARCH ARTICLE

Electrochemical Quartz Crystal Microbalance/Pt: Dissolution and oxidation of platinum thin films were measured in acidic and alkaline electrolytes with varying potential cycling ranges using electrochemical quartz crystal microbalance.

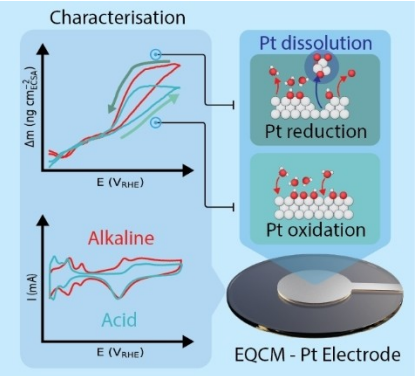

L. Strandberg, Dr. V. Shokhen, Dr. M. Luneau, Prof. G. Lindbergh, Prof. C. Lagergren, Prof. B. Wickman**

1 – 10

Comparison of Oxygen Adsorption and Platinum Dissolution in Acid and Alkaline Solutions Using Electrochemical Quartz Crystal Microbalance